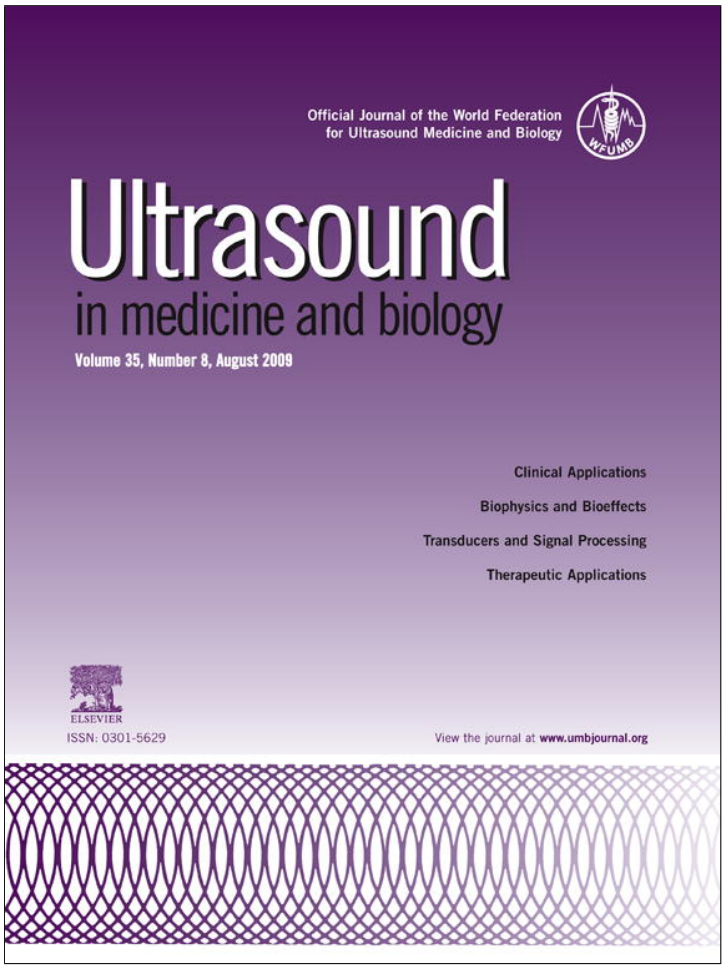

Ultrasound in Med. & Biol., Vol. 35, No. 8, pp. 1385–1396, 2009

0301-5629/09/$–see front matter

ELSEVIER

doi:10.1016/j.ultrasmedbio.2009.04.010

● *Original Contribution*

GROWTH AND DISSOLUTION OF AN ENCAPSULATED CONTRAST MICROBUBBLE: EFFECTS OF ENCAPSULATION PERMEABILITY

KAUSIK SARKAR, AMIT KATIYAR, and PANKAJ JAIN
Department of Mechanical Engineering, University of Delaware, Newark, DE

(*Received* 4 *September* 2008, *revised* 1 *April* 2009, *in final form* 16 *April* 2009)

Abstract—Gas diffusion from an encapsulated microbubble is modeled using an explicit linear relation for gas permeation through the encapsulation. Both the cases of single gas (air) and multiple gases (perfluorocarbon inside the bubble and air dissolved in surrounding liquid) are considered. An analytical expression for the dissolution time for an encapsulated air bubble is obtained; it showed that for small permeability the dissolution time increases linearly with decreasing permeability. A perfluorocarbon-filled contrast microbubble such as Definity® was predicted to experience a transient growth because of air infusion before it dissolves in conformity with previous experimental findings. The growth phase occurs only for bubbles with a critical value of initial mole fraction of perfluorocarbon relative to air. With empirically obtained property values, the dissolution time of a 2.5-micron diameter (same as that of Definity), lipid-coated octafluoropropane bubble, with surface tension 25 mN/m, is predicted to be 42 min in an air-saturated medium. The properties such as shell permeability, surface tension and relative mole fraction of octafluoropropane are varied to investigate their effects on the time scales of bubble growth and dissolution, including their asymptotic scalings where appropriate. The dissolution dynamics scales with permeability, in that when the time is nondimensioanlized with permeability, curves for different permeabilities collapse on a single curve. Investigation of bubbles filled with other gases (nonoctafluoropropane perfluorocarbon and sulfur hexafluoride) indicates longer dissolution time because of lower solubility and lower diffusivity for larger gas molecules. For such micron-size encapsulated bubbles, lifetime of hours is possible only at extremely low surface tension (<1 mN/m) or at extreme oversaturation. (E-mail: sarkar@udel.edu) © 2009 World Federation for Ultrasound in Medicine & Biology.

Key Words: **Microbubble, Ultrasound contrast agents, Dissolution, Permeability, Encapsulation, Epstein-Plesset, Gas transport.**

INTRODUCTION

Encapsulated microbubbles are used for improved contrast of ultrasound images (Chang et al. 1996; Dejong et al. 1992, 1994; Dejong and Hoff 1993; Ferrara et al. 2007; Klibanov et al. 2006; Pollard et al. 2004; Simpson et al. 1999) and drug and gene delivery (Klibanov 2006; Price et al. 1998; Shohet et al. 2000). The encapsulation, typically made of proteins, lipids and other surface active materials, stabilizes a bubble against dissolution in the bloodstream. A stable microbubble with good scattering characteristics is critical for achieving good image contrast. Dissolution of free bubbles has been investigated in detail since the pioneering study of Epstein and Plesset (1950), where they showed that an air bubble's growth (dissolution) in oversaturated (undersaturated) liquid is modified by the surface tension (see Duncan and Needham (2004) for a review of the literature). Surface tension generates a higher pressure inside the bubble, and the equation of state for the gas predicts a higher gas concentration there. Consequently, a higher gas concentration at the bubble wall drives the outward diffusion of gas in the liquid. In pure water, micron-size free air bubbles would dissolve in 30 ms (see eqn (13)), whereas an encapsulated microbubble would last much longer depending on the surface properties. Replacing air with sparingly soluble perfluorocarbon (PFC) gas (also called osmotic agent) has also contributed to increased lifetime of these bubbles (Ferrara et al. 2007).

Here we develop a mathematical model for the effects of encapsulation, incorporate it into the boundary value problem of gas diffusion, and investigate resulting bubble dynamics in the presence of perfluorocarbon inside and air dissolved in the liquid outside (air could also be

Address correspondence to: Kausik Sarkar, 126 Spencer Lab, Department of Mechanical Engineering, University of Delaware, Newark, DE 19716. E-mail: sarkar@udel.edu

Nomenclature

C	Concentration of the gas (mol m^{-3})	L_g	Ostwald coefficient
C_g	Concentration of the gas in the bubble (mol m^{-3})	L_A	Ostwald coefficient of air
C_w	Concentration of the gas at the inner wall of encapsulation (mol m^{-3})	L_F	Ostwald coefficient of OFP
C_A	Concentration of the air in the bubble (mol m^{-3})	m	Mass of the gas inside the bubble (kg)
C_F	Concentration of the OFP in the bubble (mol m^{-3})	p_{atm}	Atmospheric pressure (kg m^{-1} s^{-2})
f	Saturation level constant	P_g	Pressure of the gas inside the bubble (kg m^{-1} s^{-2})
h_g	Permeability of gas through the membrane (m s^{-1})	p_A	Partial pressure of air inside the bubble (kg m^{-1} s^{-2})
h_A	Permeability of air through the membrane (m s^{-1})	p_F	Partial pressure of OFP inside the bubble (kg m^{-1} s^{-2})
h_F	Permeability of OFP through the membrane (m s^{-1})	R	Bubble radius (m)
k_g	Coefficient of gas (air/OFP) diffusivity through the liquid (m^2 s^{-1})	R_0	Initial bubble radius (m)
k_g^e	Coefficient of gas (air/OFP) diffusivity through the membrane (m^2 s^{-1})	R_G	Universal gas constant (kg m^2 s^{-2} $mol^{-1}K^{-1}$)
k_A	Coefficient of diffusivity of the air through the liquid (m^2 s^{-1})	X_F	mole fraction of a gas in the bubble
k_F	Coefficient of diffusivity of the OFP through the liquid (m^2 s^{-1})	r	Radial distance (m)
		t	Time (s)
		T	Temperature (K)
		α	Non-dimensional number involving diffusivity, permeability and R_0
		γ	Surface tension (kg s^{-2})
		δ	Shell thickness (m)
		λ	Ratio of the diffusivities of air and OFP
		τ	Non-dimensional time

initially present inside the microbubble). This investigation is motivated by our investigation of Definity (Bristol Myers Squibb Medical Imaging, N. Billerica, MA, USA) destruction process (Chatterjee et al. 2005). Under ultrasonic excitation, we saw an increase in total attenuation from a Definity solution with time for relatively low levels of excitations, the maximum being reached around ~10 min. We inferred that the encapsulation becomes slightly permeable and leads to initially more inward diffusion of air than outward diffusion of less soluble octafluoropropane (OFP). The increased bubble size causes the increased attenuation. At intermediate excitation levels, attenuation decreased with time with decrease-rate increasing with excitation level; it indicates a far larger permeability, where outward diffusion of OFP becomes the limiting step leading to slow dissolution of bubbles. At even higher levels of excitation, attenuation decreased at a much faster rate, and the rate did not depend on excitation level, indicating a total destruction of the encapsulation. Both at intermediate and higher values of excitation, the time scale for the process was ~6–10 minutes. Such transient growth (also with 5- to 10-min time scale) was inferred by Shi and Forsberg (2000), when they observed a shift in the maximum of the attenuation spectrum of ultrasound from Optison (GE Healthcare, Princeton, NJ, USA) agent. Guan and Matula (2004) in their investigation of Sonazoid (GE Healthcare, Oslo, Norway) under ultrasonic pulse excitation and Chen et al. (2002) in their destruction study of Optison and biSphere^{TM} (POINT Biomedical, San Carlos, CA, USA) observed a temporary increase in scattered signals. They used a model developed by Kabalnov et al. (1998b). The model is an adapted version of the one developed by Epstein and Plesset (1950) for presence of both air and PFC. Kabalnov et al. (1998a, 1998b) showed that diffusivity and solubility critically affect the lifetime of contrast microbubbles. These models of contrast microbubbles did not account for the effects of encapsulation.

Recently, Duncan and Needham (2004) performed a careful test of the Epstein-Plesset dissolution model using an air bubble (of radius ~15 μm) supported on a micropipette. They concluded that the model predicts bubble dissolution time to ~10% accuracy. There has not been any model to take into account the effect of encapsulation for air bubble except for the one by Borden and Longo (2002) (the same model was also discussed in the review article by Ferrara et al. (2007)), where they assumed an additional resistance because of a shell of lipid

monolayer for the bubble (of radius ~25 μm) and incorporated it along with the resistances as a result of a polyethylene glycol (PEG) layer and the surrounding water. We see later that our model can be used to obtain the shell resistance parameter R_{shell}.

In this work we first develop a model for the effects of an encapsulation on the gas diffusion. In the subsequent subsections, we develop the single and multiple gas cases in presence of encapsulation. Wherever possible, theoretical results are related with those presented elsewhere. We then concentrate on a bubble representative of Definity contrast agent (2.5-micron diameter and containing octafluoropropane). It has a lipid encapsulation; lipid coating and gas permeation through it have been investigated quite extensively recently, making it an excellent choice for finding how the property values determine its lifetime and dissolution. The material properties such as diffusivities, Ostwald coefficients of air and octafluoropropane are determined from the literature. We investigate the time-varying behavior and dissolution time. Later, we present a parametric study of the effects of variation in surface tension, permeability, radius, Ostwald coefficient and air saturation on dissolution time. We also investigate the effects of different gas contents—perfluorocarbons and sulfur hexafluoride. We discuss our results and its implications on contrast microbubbles. The final section summarizes our findings.

MATHEMATICAL FORMULATION

Gas diffusion through permeable shell

For an encapsulated bubble, the dissolution time is much longer than the time scale for diffusion R_0/h_g through the encapsulation, where R_0 is the initial bubble radius and h_g is the permeability of gas through the membrane (see also Nomenclature for symbols). Thus, a pseudo-steady state can be assumed. Neglecting the fast transients and the convective transport term, the gas concentration C in moles/volume outside the bubble of radius R satisfies the steady-state diffusion equation, which in spherically symmetric case is

$$\frac{\partial}{\partial r}\left(r^2\frac{\partial C}{\partial r}\right)=0, \tag{1}$$

with boundary condition $C\to C(\infty)$ at $r\to\infty$ where $C(\infty)$ is the concentration of the dissolved gas in the liquid far away from the bubble (Fig. 1). The boundary condition at the liquid side of the bubble wall is that the flux in the liquid side is matched by the diffusion through the membrane. The diffusion through the membrane is modeled as proportional to the concentration difference across the membrane $C_w-C(R)$, where C_w is the gas concentration at the inner wall of the membrane in contact with the gas inside (Fig. 1) :

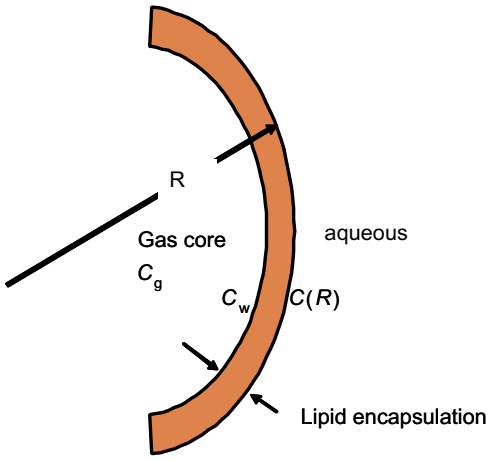

Fig. 1. Schematic for an encapsulated microbubble.

$$-k_g\left.\frac{\partial C}{\partial r}\right|_R=h_g[C_w-C(R)] \tag{2}$$

Here k_g is the coefficient of diffusivity of the gas through the liquid. The mass flux through the encapsulation is modeled by a coefficient h_g which can be thought of as $h_g\approx k_g^e/\delta$, where k_g^e is the diffusivity of the gas through the encapsulation and δ, the thickness of encapsulation. However, Fickian diffusion might be inappropriate for a monolayer encapsulation. An energy barrier model of gas permeation through membrane would also give rise to such a linear relation (Blank and La Mer 1962; Borden and Longo 2002). Solving eqn (1) with boundary condition of eqn (2), we obtain

$$C(r)=\frac{R^2(C_w-C(\infty))}{r\left(\frac{k_g}{h_g}+R\right)}+C(\infty). \tag{3}$$

The bubble contains gas at a concentration C_g. Its growth is determined by the mass flux at the bubble wall

$$\frac{dm}{dt}=\frac{d}{dt}\left(\frac{4}{3}\pi R^3C_g\right)=4\pi R^2k_g\left.\frac{\partial C}{\partial r}\right|_R. \tag{4}$$

We assume that the membrane is completely hydrated. Therefore, the dissolved gas concentration C_w at the membrane wall in contact with the inside gas is related to the inside gas concentration by the Ostwald coefficient L_g:

$$C_w=L_gC_g. \tag{5}$$

Note that for an ideal gas, it is equivalent to Henry's law, $C_w=H_D^{-1}p_g$, (H_D is Henry's constant) that relates the wall concentration to the gas partial pressure p_g. The partial pressure in turn is proportional to the concentration C_g by the gas law, giving rise to

$$L_g = H_D^{-1} R_G T, \tag{6}$$

where T and R_G are temperature and the universal gas constant. Using eqn (3), we obtain for the evolution of bubble radius:

$$\frac{d\left(R^3 C_g\right)}{dt} = 3R^2 k_g \frac{\left(C(\infty) - L_g C_g\right)}{\left(\frac{k_g}{h_g} + R\right)}. \tag{7}$$

Single gas

For a single gas content such as air, we investigate the behavior of the bubble for both cases when the gas is air (identical to the case considered by Epstein and Plesset (1950) except for the effect of the shell) or other low solubility gas such as perfluorocarbons. $C(\infty)$ is determined by the level of saturation of the liquid, with the gas at the atmospheric pressure, *i.e.*,

$$C(\infty) = f L_g p_{\text{atm}} / R_G T. \tag{8}$$

The factor f describes whether the liquid is saturated ($f=1$), undersaturated ($f<1$) or oversaturated ($f>1$) with the gas. The pressure inside the bubble is higher than the atmospheric pressure by the Laplace pressure because of surface tension γ:

$$p_g = C_g R_G T = p_{\text{atm}} + \frac{2\gamma}{R}, \qquad C_g = \frac{p_{\text{atm}}}{R_G T} + \frac{2\gamma}{R R_G T}. \tag{9}$$

Replacing $C(\infty)$ and C_g (from eqn (9)) in eqn (7) we obtain:

$$\frac{dR}{dt} = -L_g \frac{1 - f + 2\gamma/(R p_{atm})}{\left(1 + \frac{4\gamma}{3R p_{atm}}\right)\left(\frac{1}{h_g} + \frac{R}{k_g}\right)}. \tag{10}$$

This is the same equation obtained by Borden and Longo (2002) (their eqn (13) when one identifies $R_{\text{shell}} = 1/h_g$); they obtained it by an entirely different consideration of various resistances in the mass diffusion circuit. (The review article by Ferrara et al. (2007) in their eqn (1.2) has a minor typographical error of 3/4 instead of 4/3 in the first factor of the denominator.) In the limit of a free bubble, $h_g \to \infty$, we obtain the familiar Epstein-Plesset equation (eqn (15) in Duncan and Needham (2004)). Note that a nonzero surface tension γ, and undersaturation ($1-f>0$) drives dissolution. Small h_g (less permeable membrane) and small L_g (low solubility) hinder bubble dissolution. One can integrate the equation, but the result is algebraically complex to provide any additional insight. However, for the saturated case ($f=1$), we obtain:

$$\frac{p_{\text{atm}}}{6\gamma k_g}\left(R^3 - R_0^3\right) + \left(\frac{p_{\text{atm}}}{4\gamma h_g} + \frac{1}{3k_g}\right) \times \left(R^2 - R_0^2\right) + \frac{2}{3h_g}(R - R_0) = -L_g t, \tag{11}$$

and

$$\tilde{t}_{diss} \equiv \frac{t_{diss}}{R_0^2/k_g} = \frac{1}{L_g}\left[\frac{p_{atm} R_0}{\gamma}\left(\frac{1}{6} + \frac{k_g}{4h_g R_0}\right) + \frac{2k_g}{3h_g R_0} + \frac{1}{3}\right], \tag{12}$$

where dissolution time t_{diss} (when bubble radius R becomes zero) is nondimensionalized by the time scale of diffusion (R^2/k_g); $\gamma/(p_{\text{atm}} R_0)$ is the nondimensional Laplace overpressure. $h_g R_0/k_g$ is the analogue of Sherwood number, which appears in convective mass transfer. It is the ratio of the resistance caused by gas diffusivity through the bulk liquid to that because of hindered permeability of the encapsulation. The dissolution time is inversely proportional to the Ostwald coefficient L_g. However note that finite permeability, *i.e.*, finite Sherwood number, destroys the inverse proportionality with the gas diffusivity k_g. In the limit of $h_g R_0/k_g \to \infty$, we obtain

$$\tilde{t}_{diss} \equiv \frac{t_{diss}}{R_0^2/k_g} = \frac{1}{L_g}\left[\frac{p_{atm} R_0}{6\gamma} + \frac{1}{3}\right], \tag{13}$$

same as in Duncan and Needham (2004). In Fig. 2, we plot the dissolution time for an encapsulated air bubble of diameter 2.5 μm as a function of encapsulation permeability. The reference permeability used is $h_g^* = 2.785 \times 10^{-5}$m/s for air through a lipid encapsulation (see Appendix and Table 1). Other property values are given in Table 1. It shows that for small h_g , the dissolution time decreases inversely with h_g, finally reaching the limiting case of eqn (13) for large enough h_g. The limiting value for the dissolution time for this 2.5-micron

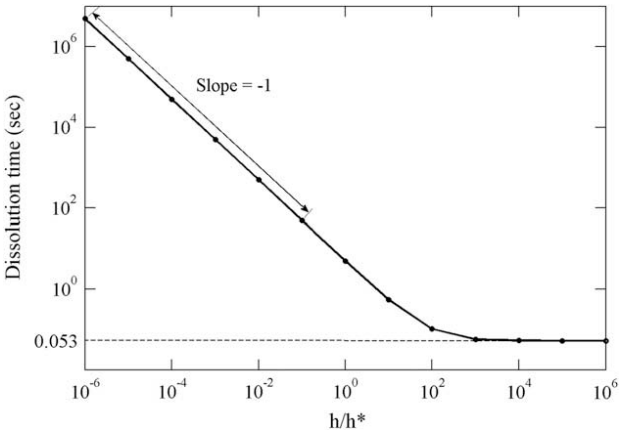

Fig. 2. Variation of dissolution time with permeability for an encapsulated 2.5-micron-diameter air bubble ,$h^* = 2.785 \times 10^{-5} m/s$.

Table 1. Physical properties of contrast microbubbles (see Appendix for references to literature and determination procedure)

Initial bubble radius (R_0)	1.25×10^{-6} m
Atmospheric pressure (p_{atm})	101325 Pa
Coefficient of diffusivity of air in water (k_A)	2.05×10^{-9} m^2 s^{-1}
Coefficient of diffusivity of SF_6 in water	1.2×10^{-9} m^2 s^{-1}
Coefficient of diffusivity of C_3F_8 in water (k_F)	7.45×10^{-10} m^2 s^{-1}
Coefficient of diffusivity of C_4F_{10} in water	6.9×10^{-10} m^2 s^{-1}
Coefficient of diffusivity of C_5F_{12} in water	6.3×10^{-10} m^2 s^{-1}
Coefficient of diffusivity of C_6F_{14} in water	5.8×10^{-10} m^2 s^{-1}
Surface tension (γ)	0.025 N/m
Ostwald coefficient of SF_6	5.4×10^{-3}
Ostwald coefficient of C_3F_8 (L_F)	5.2×10^{-4}
Ostwald coefficient of C_4F_{10}	2.02×10^{-4}
Ostwald coefficient of C_5F_{12}	1.17×10^{-4}
Ostwald coefficient of C_6F_{14}	2.3×10^{-5}
Ostwald coefficient of air (L_A)	1.71×10^{-2}
Permeability of air through the encapsulation (h_A)	2.857×10^{-5} m s^{-1}
Permeability of SF_6 through the encapsulation	8.7×10^{-6} m s^{-1}
Permeability of C_3F_8 through the encapsulation (h_F)	1.2×10^{-6} m s^{-1}
Permeability of C_4F_{10} through the encapsulation	2.57×10^{-7} m s^{-1}
Permeability of C_5F_{12} through the encapsulation	9.04×10^{-8} m s^{-1}
Permeability of C_6F_{14} through the encapsulation	4.44×10^{-8} m s^{-1}

encapsulated air bubble is 53 ms. Note that using an encapsulation with $h_g = 2.785 \times 10^{-5}$m/s increases the dissolution time to 5 s (a 100-fold increase in lifetime). The analytical expression, eqn (12), of dissolution for a single gas clearly shows the importance of the permeability barrier of the encapsulation, in that the effects of permeability adds two terms that are inversely proportional to the Sherwood number $O(k_g/h_g R)$, which is ~100 (from Table 1). The relatively moderate value of the inverse of the Sherwood number indicates that the resistance caused by the encapsulation dominates over the one caused by diffusivity through bulk liquid. In Fig. 3, we plot the dissolution time as a function of R_0 , with property values from Table 1. The rate of increase of dissolution time with initial radius is steeper than linear. For example an increase from 2–20 micron in bubble radius approximately increases the dissolution time by 100.

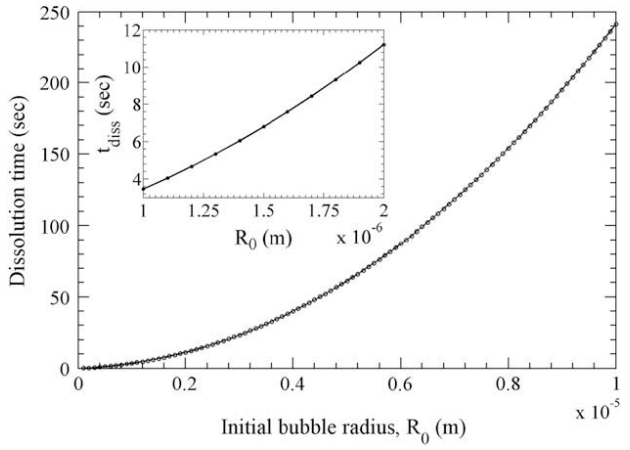

Fig. 3. Variation of dissolution time with initial radius for an encapsulated microbubble of air. *Inset*, a shorter range (1 to 2 μ) in radius variation.

Multiple gas content

The previous analysis indicates that using a gas with lower solubility and diffusivity will result in enhanced microbubble stability, as is indeed the case with the second-generation contrast microbubbles made with perfluorocarbon. The non-air filling gas is often called an osmotic agent. However, because of the presence of air dissolved in the liquid outside, air also plays a role in the dynamics. We therefore consider diffusion of two components: air A and the sparingly soluble perfluorocarbon F. One correspondingly gets two equations for these two components. We assume $C_F(\infty)=0$, *i.e.*, the gas is only introduced into the liquid through the bubbles, but $C_A(\infty)$ is determined by the fact that the liquid is in contact with air at atmospheric pressure p_{atm}, i.e., $C_A(\infty)=fL_A p_{\text{atm}}/R_G T$, as in eqn (8). The factor f as before determines the air saturation level of the liquid. The two equations are then

$$\frac{d(R^3 C_F)}{dt} = -3Rk_F \frac{L_F C_F}{\left(\frac{k_F}{h_F R}+1\right)}, \tag{14}$$

and

$$\frac{d(R^3 C_A)}{dt} = 3Rk_A L_A \frac{\left(f\frac{p_{\text{atm}}}{R_G T} - C_A\right)}{\left(\frac{k_A}{h_A R}+1\right)}. \tag{15}$$

For a free bubble $h_{A,F} \to \infty$ or, more appropriately, the nondimensional number $h_{A,F}R/k_{A,F} \to \infty$, we obtain the same equations of Kabalnov et al. (1998b) in absence of the encapsulating membrane. The pressure inside the bubble arises from partial pressures because of the osmotic agent and the air:

$$p_A + p_F = (C_A + C_F)R_G T = p_{\text{atm}} + \frac{2\gamma}{R}. \tag{16}$$

We nondimensionalize various variables (Kabalnov et al. 1998b):

$$\widehat{\gamma} = \frac{2\gamma}{p_{atm} R_0}, \ \widehat{R} = \frac{R}{R_0}, \ \lambda = \frac{k_A}{k_F}, \ \alpha_F = \frac{k_F}{h_F R_0}, \ \alpha_A = \frac{k_A}{h_A R_0},$$

$$A = \widehat{R}^3 \frac{C_A R_G T}{p_{atm}}; \ F = \widehat{R}^3 \frac{C_F R_G T}{p_{atm}}; \ \tau = \frac{k_F}{R_0^2} t,$$

where R_0 is the initial bubble radius. Eqns (14), (15) and (16) become

$$\frac{dF}{d\tau}=\frac{-3L_F F}{\widehat{R}\left(\alpha_F+\widehat{R}\right)} \tag{17}$$

$$\frac{dA}{d\tau}=\frac{-3\lambda L_A\left(A-f\widehat{R}^3\right)}{\widehat{R}\left(\alpha_A+\widehat{R}\right)}, \tag{18}$$

$$F+A=\widehat{R}^3+\widehat{\gamma}\widehat{R}^2. \tag{19}$$

Using the constraint (19) we eliminate F to obtain

$$\frac{d\widehat{R}}{d\tau}=\frac{-3}{\left(3\widehat{R}^3+2\gamma\widehat{R}^2\right)}\left\{\frac{\lambda L_A\left(A-f\widehat{R}^3\right)}{\left(\alpha_A+\widehat{R}\right)}+\frac{L_F\left(\widehat{R}^3+\widehat{\gamma}\widehat{R}^2-A\right)}{\left(\alpha_F+\widehat{R}\right)}\right\}. \tag{20}$$

Corresponding initial conditions are

$$\widehat{R}_0=1,\qquad A(0)+F(0)=\widehat{R}_0+\widehat{\gamma}\widehat{R}_0,\qquad \frac{F(0)}{A(0)+F(0)}=X_F, \tag{21}$$

where X_F is the initial mole-fraction of the insoluble gas F. One arrives at

$$A(0)=(1-X_F)\left(\widehat{R}_0+\widehat{\gamma}\widehat{R}_0\right),\qquad F(0)=X_F\left(\widehat{R}_0+\widehat{\gamma}\widehat{R}_0\right). \tag{22}$$

MATERIAL PROPERTIES

As a reference case, we take an Food and Drug Administration–approved ultrasound contrast agent, Definity. Definity microbubbles contain Octafluoropropane (OFP; n-C_3F_8) and have a fairly narrow radius distribution, with a mean diameter of 2.5 micron (Quaia 2005; Sboros et al. 2001). They have a lipid (DPPA, DPPC, MPEG5000 DPPE) encapsulation. An interfacial tension value of 0.025 N/m reduced from its pure air-water interface value of 0.072 N/m is assumed for the lipid monolayer (Duncan and Needham 2004). Note that for C16 lipids, the collapse phase surface tension was measured as 0.010 N/m (Borden and Longo 2002). The exact value of the surface tension for the encapsulation is hard to determine, especially for a micron-sized bubble. Recently, we developed an inverse procedure to measure such interfacial rheological properties (Chatterjee and Sarkar 2003; Sarkar et al. 2005). We also note that by suitably choosing the encapsulation, one can completely eliminate surface tension for a waxy solidlike layer (Duncan and Needham 2004; Kim et al. 2003). Later in this paper, we investigate the effects of surface tension variation. The values of diffusivities $k_{A,F}$ of air and OFP are provided in Table 1. Determining the value of permeability $h_{A,F}$ poses difficulty. Fickian model assumes $h_g \approx k_g^e/\delta$, which requires accurate estimation of diffusivity through the encapsulation material and the encapsulation thickness. The thickness of the Definity encapsulation has been reported with wide variation: 1–2 nm (Goertz et al. 2007), 4 nm (Chen et al. 2004) and a much larger value of 15 nm (Cheung et al. 2008). Encapsulation thickness varies between contrast microbubbles, *e.g.*, 15 nm for Optison (Christiansen et al. 1994), 200–300 nm for Quantison and 600–1000 nm for Myomop (Quaia 2005). The air diffusivity in bulk lipid is 10^{-14} m^2/s, giving $h_g \sim 10^{-5}$ m/s for $\delta \sim 1$ nm, which seems more appropriate for a lipid monolayer (Borden and Longo 2002). On the other hand, for a thin monolayer, a continuum description of diffusion through a finite layer with bulk material properties may not be appropriate. The monolayer acts more like a barrier, which only sufficiently energetic gas molecules can overcome. Such an energy barrier model for gas penetration through a thin layer has been developed by Blank (1962, 1964), Borden and Longo (2004) and Borden et al. (2006). The energy barrier depends on the gas molecules' collision diameter and surface pressure, the latter being determined by the constituent surface active molecule's geometry and packing in the layer. The resistance consequently becomes an exponential function (through the Arrhenius factor) of the layer thickness as opposed to a linear one characteristic of Fickian diffusion. Borden and Longo (2002) investigated such dependence by varying the chain length of encapsulation molecules. However, the measurement failed to conclusively determine in favor of either the Fickian diffusion

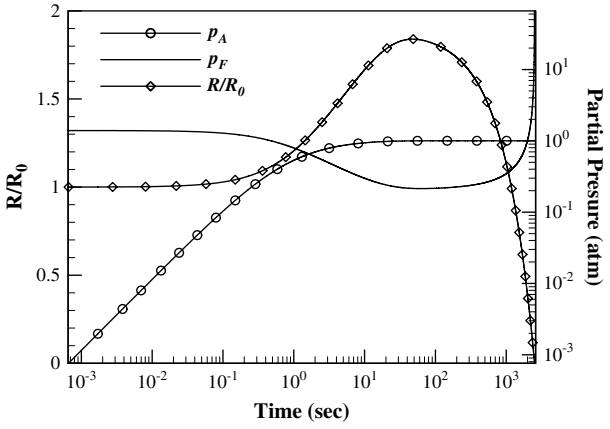

Fig. 4. Dissolution of an encapsulated 2.5-micron-diameter OFP bubble in an air-saturated medium.

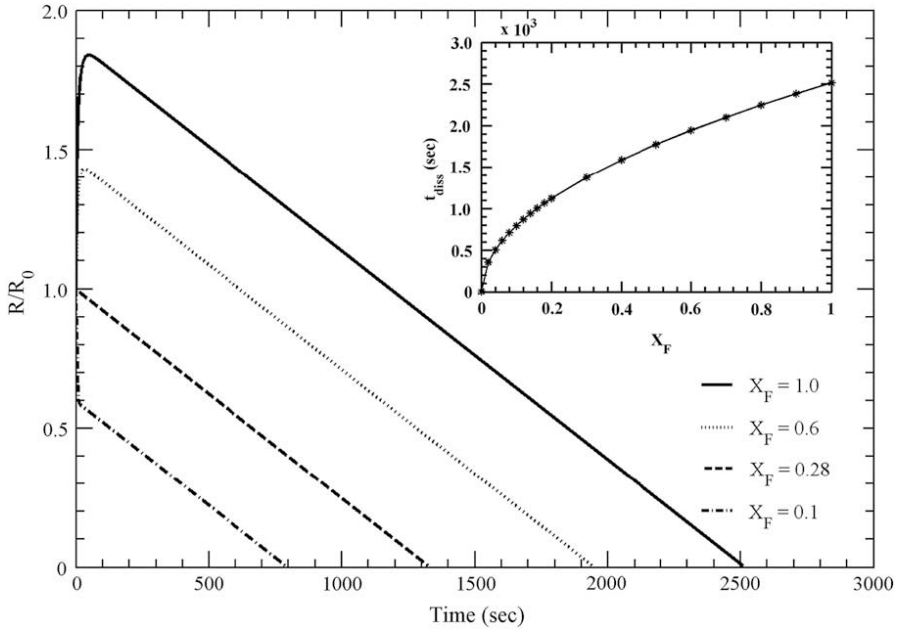

Fig. 5. Variation of R/R_0 with time for different OFP mole fractions. *Inset*, dissolution time *vs*. OFP mole fraction.

or the energy barrier model. We use the energy barrier model for determining the values of encapsulation permeability. The values are found in the Appendix to be $h_A = 2.857 \times 10^{-5}$m/s, $h_F = 1.2 \times 10^{-6}$m/s. The other parameters are listed in Table 1. The procedure for determining the properties are detailed in the Appendix. These are used except when explicitly stated otherwise. Note that both the models of gas permeation give permeability values of the same order of magnitude. Note that the encapsulation is characterized mechanically only by a surface tension—Newtonian interfacial rheology (Chatterjee and Sarkar 2003). A more complex interfacial rheology will introduce other interfacial parameters (Katiyar et al. 2009; Sarkar et al. 2005).

RESULTS AND DISCUSSION

As can be seen by the nondimensional eqns (17)–(22), the dependent variables $\widehat{R}(\tau), F(\tau)$ and $A(\tau)$ are functions of nondimensional variables $\widehat{R}_0, \widehat{\gamma}, L_F, L_A, \lambda, \alpha_F, \alpha_A$ and X_F. We present our results in terms of dimensional quantities for ease of use. MATLAB (The MathWorks, Natick, MA, USA) was used to solve the system of equations. Figure 4 shows the dissolution of a Definity microbubble with properties inferred as mentioned before (Table 1). The bubble initially grows to a maximum and then experiences slow dissolution. Note that the logarithmic time scale, used to delineate the transient dynamics exaggerates the transient time scale (see Fig. 5). The bubble reaches the maximum around 50 s and the total dissolution time is approximately 2500 s. The initial growth of the bubble is the result of more air diffusing into the bubble than OFP coming out, which in turn is because of the higher diffusivity of air than that of OFP. The temporary growth of contrast microbubbles was previously inferred from acoustic experiments, albeit under acoustic excitation (Chatterjee et al. 2005; Shi and Forsberg 2000). The predicted time scale of growth ~2 min is of the same order as the experimentally inferred one (~10 min) at low acoustic excitation. The total dissolution time as well is of the same order as that observed under intermediate and higher acoustic excitations. It indicates that acoustic excitation degrades the encapsulation, making way for the increased gas transfer. In such a process, encapsulation permeability plays a critical role in determining the bubble behavior.

Figure 4 also plots the partial pressures of air and OFP. The partial air pressure inside the bubble increases rapidly to the value of the atmospheric pressure outside, at which point the right-hand side of eqn (15) becomes zero. The partial pressure of OFP first decreases as OFP diffuses out and air diffuses into the bubble, but then it rises explosively in the final phase as the bubble radius shrinks to zero. Kabalnov et al. (1998b) predicted a lifetime of 40 s for a perfluorobutane (n-C_4F_{10}) –filled unencapsulated bubble of radius 2.5 micron (Kabalnov et al. 1998b). The OFP-filled Definity bubble, despite having half the size and a smaller perfluorocarbon, has an approximately 60 times longer lifetime, primarily because of the encapsulation.

Figure 5 shows the bubble evolution as a function of initial mole fraction of OFP. The bubble's initial growth is controlled by the initial composition of gases in the bubble; as the amount of initial air fraction increases, the initial growth of the bubble reduces, being almost zero for the

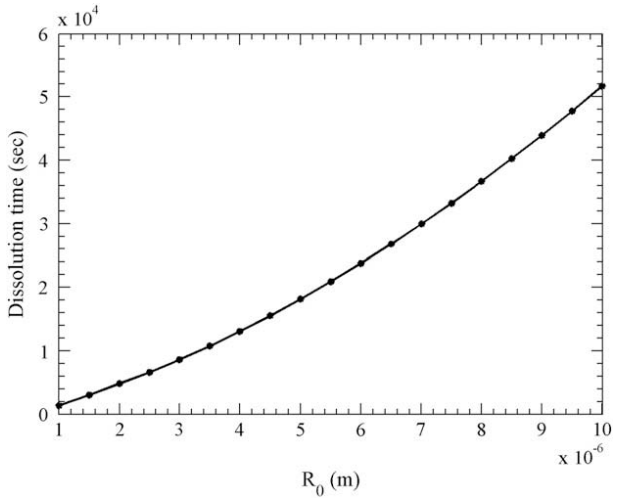

Fig. 6. Variation of dissolution time with initial bubble radius of an encapsulated OFP microbubble.

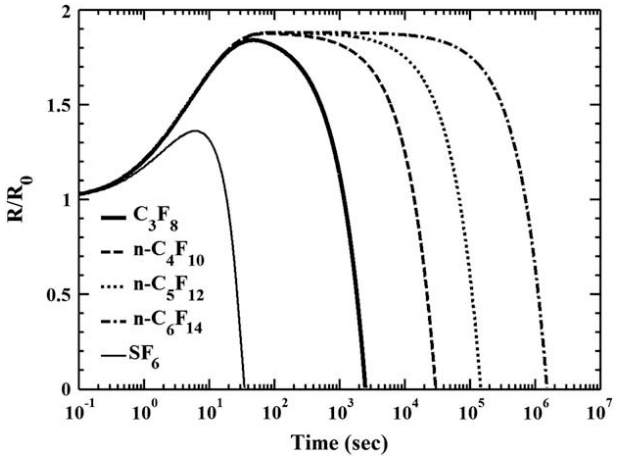

Fig. 7. Variation of R/R_0 with time for an encapsulated 2.5-micron-diameter bubble with different gas content in an air-saturated medium.

mole fraction of 0.28. For lower initial OFP content, the radius first decreases sharply for a short time interval, and after the air partial pressure inside reaches its equilibrium value of the atmospheric pressure, more gradually. In the inset, the dissolution time is seen to vary significantly with initial OFP content, especially for an air bubble ($X_F = 0$) with small addition of OFP. In the presence of sparingly soluble OFP, diffusion of air is dominated by the slower diffusion of OFP, and a higher dissolution time is observed. Figure 6 shows the effects of initial radius distribution of Definity on any particular bubble's dissolution behavior. The dissolution time increases sharply with bubble radius similar to the behavior seen for the air bubble in Fig. 3.

We then consider bubbles containing nonbranched perfluorocarbon gas other than octafluoropropane—C_4F_{10}, C_5F_{12} and C_6F_{14}—and sulfur hexafluoride (SF_6). SF_6 has been used as an osmotic agent in experimental contrast agents such as BR1 (Schneider et al. 1995) and ST44 (Forsberg et al. 1999). The gas properties are listed in Table 1; some are taken from Kabalnov et al. (1998b) (their Table 1 had a typographical error in the diffusion coefficient unit—$D \times 10^{10} m^2/s$—revealed when values are calculated from their Appendix). The properties for SF_6 listed in Table 1 are found from previous measurements (see Appendix). SF_6 is the smallest molecule, with correspondingly largest diffusivity, permeability and solubility. Therefore, in Fig. 7, it shows the shortest dissolution time. For perfluorocarbons, with increasing carbon chain length, solubility, diffusivity and permeability are reduced, leading to increased dissolution time; they show similar growth and dissolution pattern. The dissolution times are reported in Table 2.

Next, we analyze the effects of other parameters such as permeability and surface tension on the dissolution behavior. We already noted the difficulties in ascertaining their values. Furthermore, under ultrasound excitation and in suspension over time, the encapsulation would show structural deterioration, resulting in different property values (Chen et al. 2002; Chomas et al. 2000; Shi and Forsberg 2000). Therefore, knowledge of the effects of property variation would be useful in interpreting experimental results and in designing better contrast agents. Figure 8 shows the dynamics of an OFP bubble in a saturated medium for different surface tension values. Nonzero surface tension *via* Laplace pressure causes the bubble to dissolve, as the inside pressure is always higher than the outside pressure driving the gradient. The zero surface tension on the other hand predicts a final nonzero radius. OFP diffuses out of the bubble, reducing its partial pressure to zero, but air diffuses into the bubble, and the bubble can finally reach a nonzero equilibrium radius when inside pressure equals the outside pressure. The inset shows the increase in dissolution time as surface tension decreases from its pure air-water interface value of 0.072 N/m. The increase is initially gradual, and only below 1 mN/m it is much sharper reaching hours of lifetime.

Figure 9a shows the effects of encapsulation permeability on bubble dissolution. For the parametric study, we

Table 2. Dissolution time for a 2.5-micron encapsulated microbubble with different gases in an air-saturated medium

Osmotic agent	Dissolution time, t_{diss}
SF_6	35 s
C_3F_8	42 min
n-C_4F_{10}	83 h
n-C_5F_{12}	17 d
n-C_6F_{14}	17 d 14 h

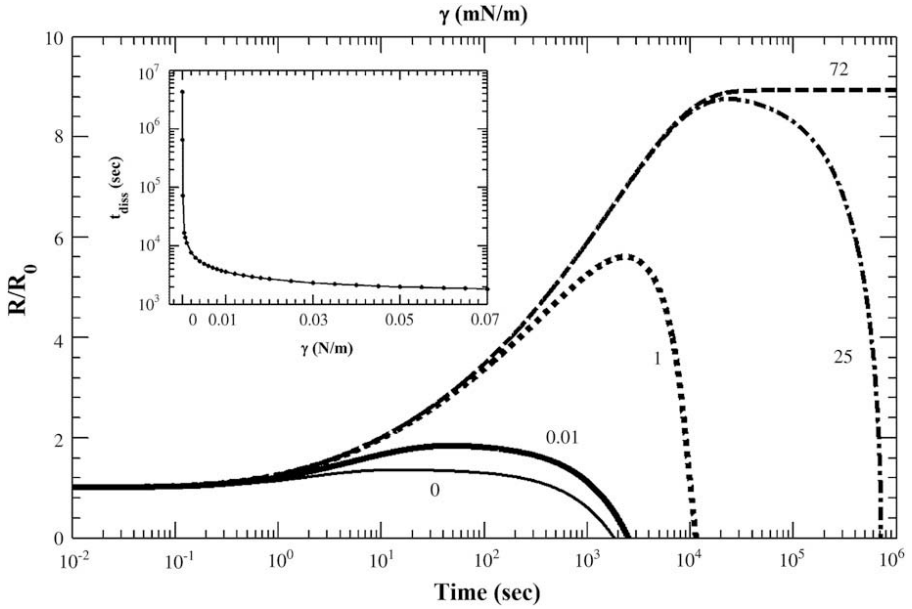

Fig. 8. Variation of R/R_0 of an encapsulated OFP microbubble with time for different surface tension values; *inset*, dissolution time variation with surface tension.

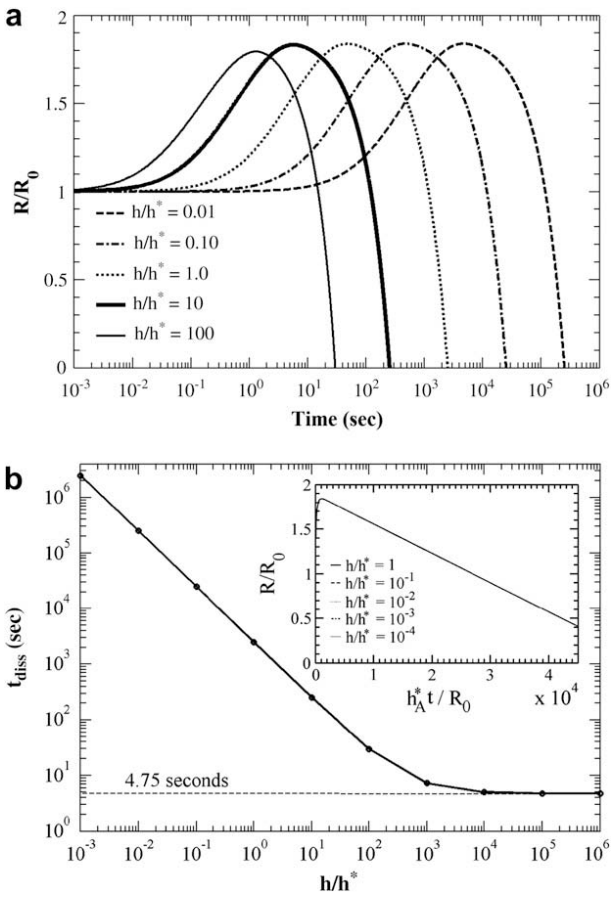

Fig. 9. (a) Variation of R/R_0 of an encapsulated OFP microbubble with time for different permeability values, $h_A^*=2.857\times 10^{-5} m/s, h_F^*=1.6\times 10^{-6} m/s$. (b) Dissolution time variation of an encapsulated OFP microbubble with permeability; *inset*, variation of R/R_0 with nondimensional time.

vary both air and OFP permeability by the same multiplicative factor assuming that air and OFP interact similarly with the encapsulation constituents. This assumption can easily be relaxed. As expected, increasing the permeability delays the growth and the dissolution process. As with the case of an air bubble in Fig. 2, the OFP bubble with very high permeability reaches the limiting value of dissolution time of about 4.75 seconds (Fig. 9b), in contrast to 53 milliseconds for an air bubble. For low permeability, the dissolution time seems to scale with permeability. Indeed when the time is scaled with permeability in the inset of Fig. 9b, all curves for different permeability (from Figure 9a) collapse on to a single curve. Figure 10 shows that there is an inverse relation between dissolution time and Ostwald coefficient as also shown by eqn (12) for single-gas bubbles, the minimum value of the coefficient in the figure being close to that of air.

We note here that only extremely low values of surface tension or unusually low encapsulation permeability would lead to a relatively stable (hours of lifetime) bubble. Typically, for the second-generation microbubbles, several hours of lifetime have been suggested. In the model presented, a nonzero surface tension and undersaturation ($1-f>0$) drive the dissolution. Undersaturation plays a role in physiological situations. We therefore study the effects of undersaturation in Fig. 11, with a surface tension value of zero. We observe that even for zero surface tension, the undersaturation is an extremely efficient mechanism for driving towards dissolution. Only for extremely low values ($\sim 10^{-3}$) of $(1-f)$, we obtain microbubble lifetime greater than a day.

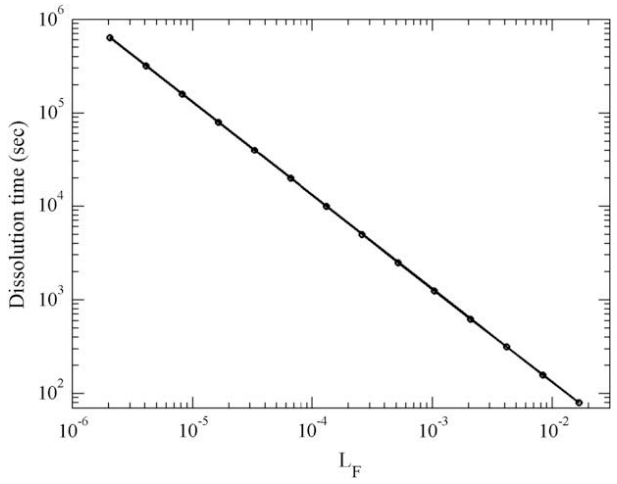

Fig. 10. Variation of dissolution time with Ostwald coefficient of osmotic agent.

SUMMARY

We have developed and investigated a new model for gas diffusion from encapsulated contrast microbubbles. A new linear permeability model is assumed for the gas diffusion through the encapsulating shell, which is appropriate for both Fickian diffusion and energy barrier models. With typical values for material constants, layer thickness and molecular parameters, both theories give rise to permeability values of the same order of magnitude.

Both air and perfluorocarbon bubbles are modeled. In the latter case, diffusion of perfluorocarbon, as well as air dissolved in the liquid, is accounted for. We have developed an analytical relation for the dissolution time of an air bubble, which shows an inverse relation with encapsulation permeability. For an air bubble, a 100-fold increase and for an OFP bubble, a 500-fold increase in dissolution time compared with free bubbles is predicted with a Definity-like encapsulation. The relative importance of the encapsulation permeability compared with bulk diffusion in determining the lifetime of an encapsulated bubble, as exemplified by the low value of Sherwood number, underscores the choice of appropriate encapsulating material for optimal design of contrast agents. The dissolution time also rises sharply with initial radius.

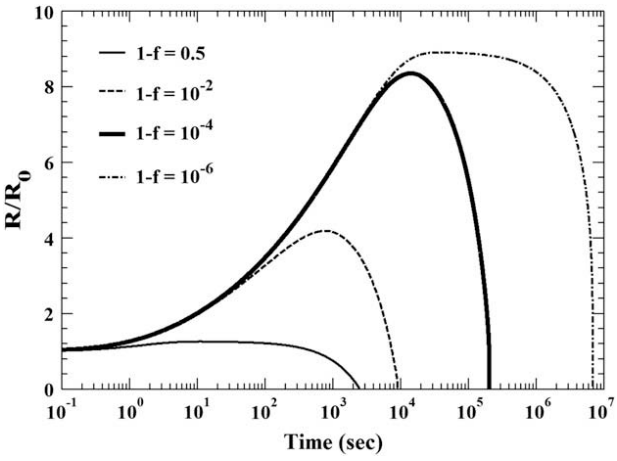

Fig. 11. Variation of R/R_0 and dissolution time with saturation level for zero surface tension.

We investigate an encapsulated octafluoropropane-filled microbubble with the physical properties representative of the Definity contrast agent. We find that such a bubble dissolves in 2500 s. But before dissolution, the bubble experiences a transient growth caused by more air going into the bubble from surrounding liquid than OFP going out. Increasing initial air content of the bubble reduces the growth part, making it negligible for OFP mole fraction of 0.28. The simulated time scales of growth and complete dissolution match in order of magnitude with what can be inferred from experiments under acoustic excitation.

The dissolution curves for different permeabilities collapse onto a single curve when the time is appropriately scaled with permeability. We also investigate the effects of the filling gas—perfluorocarbons of increasing chain length and sulfur hexafluoride. Increased size of gas molecule results in lower water solubility and lower diffusivity, both through encapsulation and water, leading to longer lifetimes. Decreasing surface tension also lengthens the lifetime, giving a stable bubble at zero surface tension. However, we note that one has to really reach extremely low surface tension before one reaches more than a few hours of lifetime. Duncan and Needham (2004) showed that solid waxy encapsulation is possible under careful preparation that has effectively a zero surface tension. It remains to be determined if the commercially available contrast agents have such an encapsulation. For a zero surface tension case, we further find that slight undersaturation is sufficient to result in reduced bubble life. Noting the difficulty in determining the material properties of the encapsulation, the parametric study presented here can be an effective tool in designing better contrast agents. Different constitutive properties of the encapsulation, with added explicit interfacial elasticity, results in different dissolution dynamics (Katiyar et al. 2009).

Acknowledgments—The authors acknowledge financial support from NSF CBET-0651912. It is also partially supported by U.S. Army Medical Research Material Command under W81XWH-08-1-0503, AHA grant no 06554414 and NIH HL081892. K.S. acknowledges fruitful discussion with Professor Mark Borden at Columbia University and Flemming Forsberg at Thomas Jefferson University.

REFERENCES

Blank M. Monolayer permeability to gases and properties of cell membranes. Fed Proc 1962;21:151.

Blank M. Approach to theory of monolayer permeation by gases. J Phys Chem 1964;68:2793.

Blank M, La Mer VK. The energy barrier for monolayer penetration. In: La Mer VK, ed. Retardation of Evaporation by Monolayers, New York: Academic Press, 1962, pp. 59-66.

Borden MA, Longo ML. Dissolution behavior of lipid monolayer-coated, air-filled microbubbles: Effect of lipid hydrophobic chain length. Langmuir 2002;18:9225–9233.

Borden MA, Longo ML. Oxygen permeability of fully condensed lipid monolayers. J Phys Chem B 2004;108:6009–6016.

Borden MA, Martinez GV, Ricker J, Tsvetkova N, Longo M, *et al*. Lateral phase separation in lipid-coated microbubbles. Langmuir 2006;22:4291–4297.

Chang PH, Shung KK, Levene HB. Quantitative measurements of second harmonic Doppler using ultrasound contrast agents. Ultrasound Med Biol 1996;22:1205–1214.

Chatterjee D, Jain P, Sarkar K. Ultrasound-mediated destruction of contrast microbubbles used for medical imaging and drug delivery. Phys Fluids 2005;17:100603.

Chatterjee D, Sarkar KA. Newtonian rheological model for the interface of microbubble contrast agents. Ultrasound Med Biol 2003;29: 1749–1757.

Chen WS, Lu XC, Liu YB, Zhong P. The effect of surface agitation on ultrasound-mediated gene transfer in vitro. J Acoust Soc Am 2004; 116:2440–2450.

Chen WS, Matula TJ, Crum LA. The disappearance of ultrasound contrast bubbles: Observations of bubble dissolution and cavitation nucleation. Ultrasound Med Biol 2002;28:793–803.

Cheung K, Couture O, Bevan PD, Cherin E, Williams R, *et al*. In vitro characterization of the subharmonic ultrasound signal from Definity microbubbles at high frequencies. Phys Med Biol 2008;53: 1209–1223.

Chomas JE, Dayton PA, May D, Allen J, Klibanov A, Ferrara K. Optical observation of contrast agent destruction. Appl Phys Lett 2000;77: 1056–1058.

Christiansen C, Kryvi H, Sontum PC, Skotland T. Physical and biochemical-characterization of Albunex™, a new ultrasound contrast agent consisting of air-filled albumin microspheres suspended in a solution of human albumin. Biotechnol Appl Biochem 1994;19:307–320.

Ciani I, Burt DP, Daniele S, Unwin PR. Effect of surface pressure on oxygen transfer across molecular monolayers at the air/water interface: Scanning electrochemical microscopy investigations using a mercury hemispherical microelectrode probe. J Phys Chem B 2004;108:3801–3809.

Dejong N, Cornet R, Lancee CT. Higher harmonics of vibrating gas-filled microspheres.1. Simulations. Ultrasonics 1994;32:447–453.

Dejong N, Hoff L. Ultrasound scattering properties of Albunex microspheres. Ultrasonics 1993;31:175–181.

Dejong N, Hoff L, Skotland T, Bom N. Absorption and scatter of encapsulated gas filled microspheres—Theoretical considerations and some measurements. Ultrasonics 1992;30:95–103.

Duncan PB, Needham D. Test of the Epstein-Plesset model for gas microparticle dissolution in aqueous media: Effect of surface tension and gas undersaturation in solution. Langmuir 2004;20:2567–2578.

Epstein PS, Plesset MS. On the stability of gas bubbles in liquid-gas solutions. J Chem Phys 1950;18:1505–1509.

Ferrara K, Pollard R, Bordeni M. Ultrasound microbubble contrast agents: Fundamentals and application to gene and drug delivery. Annu Rev Biomed Eng 2007;9:415–447.

Ferrell RT, Himmelblau DM. Diffusion coefficients of nitrogen and oxygen in water. J Chem Eng Data 1967;12:111–115.

Forsberg F, Basude R, Liu JB, Alessandro J, Shi WT, *et al*. Effect of filling gases on the backscatter from contrast microbubbles: Theory and in vivo measurements. Ultrasound Med Biol 1990;25: 1203–1211.

Goertz DE, de Jong N, van der Steen AFW. Attenuation and size distribution measurements of definity (TM) and manipulated definity (TM) populations. Ultrasound Med Biol 2007;33:1376–1388.

Guan JF, Matula TJ. Using light scattering to measure the response of individual ultrasound contrast microbubbles subjected to pulsed ultrasound in vitro. J Acoust Soc Am 2004;116:2832–2842.

Hayduk W, Laudie H. Prediction of diffusion-coefficients for nonelectrolytes in dilute aqueous-solutions. Aiche J 1974;20:611–615.

Kabalnov A, Bradley J, Flaim S, Klein D, Pelura T, *et al*. Dissolution of multicomponent microbubbles in the bloodstream: 2. Experiment. Ultrasound Med Biol 1998a;24:751–760.

Kabalnov A, Klein D, Pelura T, Schutt E, Weers J. Dissolution of multicomponent microbubbles in the bloodstream: 1. Theory. Ultrasound Med Biol 1998b;24:739–749.

Kabalnov AS, Makarov KN, Shcherbakova OV. Solubility of fluorocarbons in water as a key parameter determining fluorocarbon emulsion stability. J Fluor Chem 1990;50:271–284.

Katiyar A, Sarkar K, Jain P. Effects of encapsulation elasticity on the stability of an encapsulated microbubble. J Colloid Interface (in press) doi:10.1016/j.jcis.2009.05.019.

Kim DH, Costello MJ, Duncan PB, Needham D. Mechanical properties and microstructure of polycrystalline phospholipid monolayer shells: Novel solid microparticles. Langmuir 2003;19:8455–8466.

King DB, Saltzman ES. Measurement of the diffusion-coefficient of sulfur-hexafluoride in water. J Geophys Res Oceans 1995;100: 7083–7088.

Klibanov AL. Microbubble contrast agents—Targeted ultrasound imaging and ultrasound-assisted drug-delivery applications. Invest Radiol 2006;41:354–362.

Klibanov AL, Rychak JJ, Yang WC, Alikhani S, Li B, *et al*. Targeted ultrasound contrast agent for molecular imaging of inflammation in high-shear flow. Contrast Media Mol Imaging 2006;1:259–266.

Lawson DD, Moacanin J, Scherer KV, Terranova TF, Ingham JD. Methods for estimation of vapor-pressures and oxygen solubilities of fluorochemicals for possible application in artificial blood formulations. J Fluorine Chem 1978;12:221–236.

Lide DR. CRC Handbook of Chemistry and Physics, 79th Edition, Boca Raton: CRC Press, 1998.

Morrison TJ, Johnstone NBB. The salting-out of non-electrolytes.3. The inert gases and sulphur hexafluoride. J Chem Soc 1955;3655–3659.

Pollard RE, Garcia TC, Stieger SM, Ferrara KW, Sadlowski AR, Wisner ER. Quantitative evaluation of perfusion and permeability of peripheral tumors using contrast-enhanced computed tomography. Invest Radiol 2004;39:340–349.

Price RJ, Skyba DM, Skalak TC, Kaul S. Delivery of colloidal particles and red blood cells to tissue through microvessel ruptures resulting from microbubble destruction by ultrasound. Circulation 1998;98: 570.

Pu G, Longo ML, Borden MA. Effect of microstructure on molecular oxygen permeation through condensed phospholipid monolayers. J Am Chem Soc 2005;127:6524–6525.

Quaia E. Classification and safety of microbubble-based contrast agents. In: Quaia E, ed. Contrast Media in Ultrasonography: Basic principles and Clinical Applications, Berlin: Springer, 2005. pp. 3-14.

Sarkar K, Shi WT, Chatterjee D, Forsberg F. Characterization of ultrasound contrast microbubbles using in vitro experiments and viscous and viscoelastic interface models for encapsulation. J Acoust Soc Am 2005;118:539–550.

Sboros V, Moran CM, Pye SD, McDicken WN. Contrast agent stability: A continuous B-mode imaging approach. Ultrasound Med Biol 2001; 27:1367–1377.

Schneider M, Arditi M, Barrau MB, Brochot J, Broillet A, *et al*. Br1—A new ultrasonographic contrast agent based on sulfur hexafluoride-filled microbubbles. Invest Radiol 1995;30:451–457.

Shi WT, Forsberg F. Ultrasonic characterization of the nonlinear properties of contrast microbubbles. Ultrasound Med Biol 2000;26:93–104.

Shohet RV, Chen SY, Zhou YT, Wang ZW, Meidell RS, Unger TH, Grayburn PA. Echocardiographic destruction of albumin microbubbles directs gene delivery to the myocardium. Circulation 2000;101: 2554–2556.

Siebert EMD, Knobler CM. Interaction Virial Coefficients in Hydrocarbon-Fluorocarbon Mixtures. Journal of Physical Chemistry 1971;75. 3863–3870.

Simpson DH, Chin CT, Burns PN. Pulse inversion Doppler: A new method for detecting nonlinear echoes from microbubble contrast agents. IEEE Transa Ultrason Ferroelectr Freq Control 1999;46: 372–382.

APPENDIX

The oxygen permeability of phospholipid monolayer as a function of domain boundary density has been determined (Pu et al. 2005). The mean value of shell resistance for oxygen through a C16 lipid monolayer is 350 s/cm. We use shell resistance of air to be the same as that of oxygen and therefore its inverse $h_A = 2.857 \times 10^{-5}$m/s. Using the energy barrier model for diffusion, the shell resistance of two gases are related to their collision diameters and the surface pressure (Blank and La Mer 1962; Ciani et al. 2004, Ferrara et al 2007):

$$\frac{R_{OFP}^{shell}}{R_{Oxygen}^{shell}} = \exp\left(\frac{\pi \Pi}{4\,k\,T}\left(a_{OFP}^2 - a_{Oxygen}^2\right)\right)$$

The collision diameters for OFP and oxygen are $a_{\mathrm{OFP}} = 6.95A^\circ$, $a_{\mathrm{Oxygen}} = 3.6A^\circ$ (Siebert and Knobler 1971). Π is the surface pressure (47 mN/m; the difference in air-water interfacial tensions for the free interface, 72 mN/m, and the adsorbed interface, 25 mN/m). We get $h_F = 1.2 \times 10^{-6}$ m/s. Similarly, we obtain permeability for nonoctafluoropropane perfluorocarbons and sulfur hexafluoride using their collision diameters from Siebert and Knobler (1971). The diffusion coefficient of air in water has been calculated to be $k_A = 2.05 \times 10^{-9}\ \mathrm{m^2 s^{-1}}$ by the molar average of the diffusivities of oxygen ($2.20 \times 10^{-9}\ \mathrm{m^2 s^{-1}}$) and nitrogen ($2.01 \times 10^{-9} m^2 s^{-1}$) at 25 °C (Ferrell and Himmelblau 1967). The diffusion coefficient of OFP in water is calculated using an empirical correlation (Hayduk and Laudie 1974; Kabalnov et al. 1998b)

$$k_F = 13.26 \times 10^{-9} \cdot V_m^{-0.589}\ \mathrm{m^2/s},$$

where V_m is the molar volume in $\mathrm{cm^3/mol}$. The molar volume of OFP is calculated using the group additive method and the molar volumes of CF_3 and CF_2 groups (Lawson et al. 1978). We find $k_F = 7.45 \times 10^{-10}\ \mathrm{m^2/s}$. The Ostwald coefficient of air is also calculated as $L_A = 1.71 \times 10^{-2}$ by the molar average of the Ostwald coefficients of nitrogen (1.448×10^{-2}) and oxygen (2.773×10^{-2}) following Lide (1998). The solubility of nonbranched fluorocarbons in the homologous series decrease by a factor of ~8 (Kabalnov et al. 1990). The solubility of OFP is then obtained by those of C_2F_6 (1.272×10^{-3}) and C_4F_{10} (2.02×10^{-4}) to be $L_F = 5.2 \times 10^{-4}$. The diffusivity of SF_6 ($1.2 \times 10^{-9}\ \mathrm{m^2\ s^{-1}}$) listed in Table 1 was obtained using a correlation provided by King and Saltzman (1995), based on their measurement, the value being very similar to the one predicted by the above correlation of Hayduk and Laudie, with $V_m = 77.69\ \mathrm{cm^3/mol}$. The Ostwald coefficient of SF_6 (5.4×10^{-3}) is measured by Morrison and Johnstone (1955).